

Hybrid Diffusion Policies with Projective Geometric Algebra for Efficient Robot Manipulation Learning

Xiatao Sun^{1†}, Yuxuan Wang², Shuo Yang², Yinxing Chen¹, Daniel Rakita^{1†}

¹Yale University ²University of Pennsylvania

[†]Corresponding authors: {xiatao.sun, daniel.rakita}@yale.edu

Abstract: Diffusion policies have become increasingly popular in robot learning due to their reliable convergence in motion generation tasks. At a high level, these policies learn to transform noisy action trajectories into effective ones, conditioned on observations. However, each time such a model is trained in a robotics context, the network must relearn fundamental spatial representations and operations, such as translations and rotations, from scratch in order to ground itself and operate effectively in a 3D environment. Incorporating geometric inductive biases directly into the network can alleviate this redundancy and substantially improve training efficiency. In this paper, we introduce hPGA-DP, a diffusion policy approach that integrates a mathematical framework called *Projective Geometric Algebra* (PGA) to embed strong geometric inductive biases. PGA is particularly well-suited for this purpose as it provides a unified algebraic framework that naturally encodes geometric primitives, such as points, directions, and rotations, enabling neural networks to reason about spatial structure through interpretable and composable operations. Specifically, we propose a novel diffusion policy architecture that incorporates the Projective Geometric Algebra Transformer (P-GATr), leveraging its $E(3)$ -equivariant properties established in prior work. Our approach adopts a hybrid architecture strategy, using P-GATr as both a state encoder and action decoder, while employing U-Net or Transformer-based modules for the denoising process. Several experiments and ablation studies in both simulated and real-world environments demonstrate that hPGA-DP not only improves task performance and training efficiency through the geometric bias of P-GATr, but also achieves substantially faster convergence through its hybrid model compared to architectures that rely solely on P-GATr.

Keywords: Imitation Learning, Geometric Algebra, Manipulation

1 Introduction

Diffusion policies [1] have emerged as a powerful paradigm for visuomotor control in robotics, offering reliable convergence through iterative denoising of action trajectories. These models are typically trained from scratch with hundreds of epochs, and while effective, this training paradigm presents a critical inefficiency: the network must repeatedly relearn basic spatial priors—such as translations and rotations—for every new task or environment. This redundant relearning not only inflates the computational cost but also slows down convergence.

Given that spatial concepts are inherently universal across robotic tasks, integrating geometric inductive biases directly into the network architecture presents a compelling strategy to alleviate this redundancy. Projective Geometric Algebra (PGA), a mathematical framework offering a unified representation of spatial entities and operations through mathematical objects called *multivectors*, is particularly suited to embedding such biases. Multivectors provide a structured algebraic and geometric representation for spatial priors like points, translations, and rotations, which enables neural networks to perform spatial computations more efficiently and intuitively, thereby potentially im-

proving training efficiency and task performance. We provide a primer for Geometric Algebra and Projective Geometric Algebra in the Appendix (§A.1–A.2).

To incorporate PGA into general learning tasks, prior research has proposed the Projective Geometric Algebra Transformer (P-GATr) [2], demonstrating its effectiveness in a set of initial spatial learning tasks, such as simulated n-body modeling and predicting shear stress in human arteries, outperforming non-geometric architectures. However, incorporating P-GATr directly as a denoising backbone within diffusion policies is challenging in robotics contexts. As our experiments suggest, the inherent geometric inductive biases and the complexity of multivector computations within P-GATr make it difficult to directly learn noise prediction for effective denoising, resulting in prohibitively slow convergence.

To overcome these limitations, we propose the **hybrid Projective Geometric Algebra Diffusion Policy (hPGA-DP)**, a hybrid diffusion policy architecture that predicts an action sequence based on an observation sequence of the concatenations of the proprioceptive states of the robot and poses of task-relevant objects. The approach is designed to leverage the strengths of both geometric and traditional neural network approaches. Specifically, we employ P-GATr as a spatial state encoder and action decoder, while utilizing established architectures such as U-Net [3] or Transformer [4] for the denoising module. This hybrid approach allows the strong geometric inductive biases of P-GATr to efficiently embed spatial structures into a representation space amenable to effective denoising, while simultaneously benefiting from the proven denoising capabilities of conventional architectures. To our knowledge, our work is the first to incorporate PGA into network architecture for diffusion policies.

We evaluate and validate hPGA-DP through several experiments and ablation studies in both simulated and real-world scenarios. Our results demonstrate that hPGA-DP successfully addresses the convergence issues observed when solely relying on P-GATr, achieving significantly faster convergence and superior task performance compared to standard Transformer or U-Net-based diffusion policy architectures.

2 Related Works

Diffusion Policy. Diffusion models, originally proposed by Ho et al. [5], generate data by reversing a stochastic forward process, and have achieved remarkable success in image and video synthesis [6, 7, 8]. These models have since been adapted for robotic motion generation, with diffusion policies becoming a prominent paradigm for robot learning [1, 9, 10, 11], albeit requiring extensive training over hundreds of epochs.

To mitigate this issue, several works aim to improve training or inference efficiency: Ze et al. [12] proposed using point clouds for richer input; Wang et al. [13] imposed symmetry in denoising to boost generalization; Sun et al. [14] exploited low-rank overparameterization to accelerate training; and Reuss et al. [15] employed mixture-of-experts to reduce inference cost.

While effective, these efforts largely target data efficiency, modality, or inference, without altering the network backbone. Prior architectural innovations centered on Transformers [16, 17, 18], yielding only modest improvements. In contrast, our hPGA-DP introduces a novel hybrid architecture that achieves substantially better training efficiency and policy performance.

Geometric Algebra for Robot Learning. Geometric Algebra (GA) offers a unified framework for representing geometric entities and transformations [19]. Among its variants, Projective Geometric Algebra (PGA) is tailored for Euclidean geometry, using planes as primitives to represent motions compactly with just four basis elements [20, 21]. While GA is mathematically mature, its adoption in robotics and machine learning remains limited, with most applications favoring Conformal Geometric Algebra (CGA) [22, 23, 24] due to its symbolic compactness, as seen in manipulation control [25] and tactile ergodic control [26].

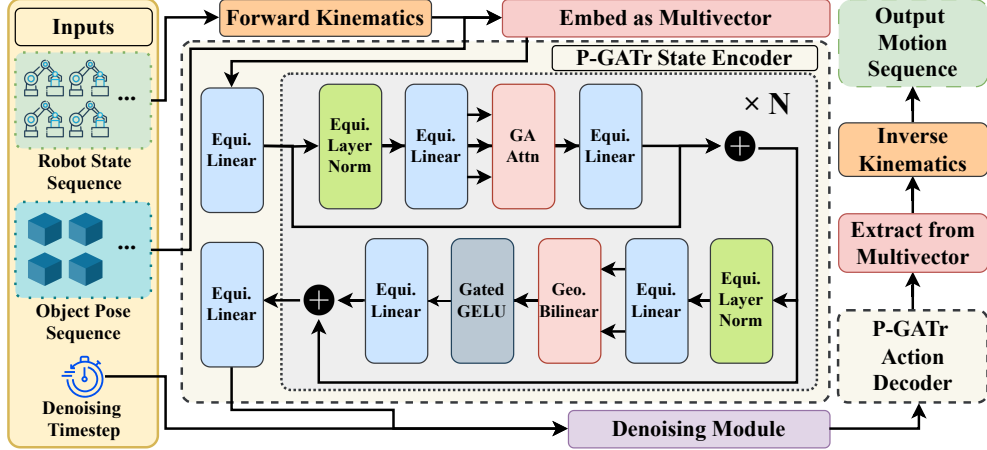


Figure 1: Overview of the hPGA-DP network architecture.

For robotics tasks grounded in Euclidean spaces, PGA ($\mathbb{G}_{3,0,1}$) offers a computationally simpler yet expressive alternative [2, 27, 28, 29]. Existing PGA applications have largely focused on dynamics modeling [30, 31], with limited exploration in learning due to the scarcity of GA-compatible neural architectures [32, 33]. The recent Projective Geometric Algebra Transformer (P-GATr) [2] addresses this gap by embedding geometric inductive biases for geometric learning [34, 35, 36].

In robotics, a concurrent work [37] applied P-GATr within diffusion models for grasp generation, but the approach is limited to static tasks and requires long training times. In contrast, our proposed hPGA-DP is an end-to-end diffusion policy architecture that achieves superior performance and faster convergence compared to baseline methods across a broad range of robotic learning tasks.

3 Technical Overview

In this section, we present an overview of our proposed hPGA-DP approach. The goal of hPGA-DP is to learn a receding horizon policy π_θ that outputs a sequence of actions $\mathbf{a}^{t:t+H_p}$ conditioned on a sequence of observations $\mathbf{o}^{t-H_o:t}$, where H_p and H_o denote the action prediction and observation horizons, respectively.

Observations. Each observation at time t is defined as $\mathbf{o}_t = [\mathbf{s}_t, \{\mathbf{T}_i^t\}_{i=1}^J]$, where $\mathbf{s}_t \in \mathbb{R}^{d_s}$ represents the robot state, and $\{\mathbf{T}_i^t\}_{i=1}^J$ denotes the spatial poses of the J task-relevant objects. Each pose \mathbf{T}_i^t consists of a 3D position vector and a unit quaternion representing orientation.

Actions. Each action at time \mathbf{a}_t may include spatial positions and/or orientations for key links on a robot or any other scalar properties that can affect change on the robot platform. For instance, an action may include the end-effector position at the given time, $\mathbf{p}_{ee}^t \in \mathbb{R}^3$, the end-effector orientation at the given time, $\mathbf{q}_{ee}^t \in \mathbb{H}_1$ (the space of unit-quaternions), and scalar representing how open or closed the gripper is at the given time $g^t \in \mathbb{R}$. The action representation is flexible and can include any number platform-specific properties, accommodating various embodiments such as bimanual or humanoid robots with multiple end-effectors. We assume that any system adopting our approach can convert these high-level actions into corresponding robot states or control commands, such as through an inverse kinematics solver.

Architecture. The network architecture for hPGA-DP is illustrated in Fig. 1. First, the robot states from the input observation sequence are converted into the positions and orientations of key links, such as end-effectors, using the robot’s forward kinematics model, in a manner similar to the action representation described above. These spatial components, combined with the poses of task-relevant objects, are then transformed into *multivectors*, the central representational objects in geometric al-

gebra. Detailed projective geometric algebra conversions from positions and orientations to multivectors are described in A.3.

The resulting multivectors are stacked in a tensor $\mathbf{x}_o^{t-H_o:t} \in \mathbb{R}^{H_o \times K_o \times 16}$, where H_o is the observation horizon, K_o is the total number positions and orientations of key links on the robot and task-relevant objects in the observations, and 16 is the length of a multivector in $\mathbb{G}_{3,0,1}$. The multivector stack is then processed by a P-GATr state encoder [2] to produce an observation latent, $\mathbf{z}_o \in \mathbb{R}^{H_o \times K_o \times 16}$. Note that this latent representation maintains the same dimensionality as the input multivector stack.

The observation latent tensor \mathbf{z}_o is passed to a denoising module, implemented as either a Transformer or U-Net, which produces denoised action latents $\mathbf{z}_a \in \mathbb{R}^{H_p \times K_a \times 16}$. Here, H_p denotes the prediction horizon, K_a is the total number of positional, rotational, or scalar components in an action, and 16 is the dimensionality of a multivector in $\mathbb{G}_{3,0,1}$. These action latents are then decoded by a P-GATr action decoder [2], which mirrors the structure of the state encoder.

The decoder produces a stack of action multivectors as a tensor $\mathbf{x}_a^{t:t+H_p} \in \mathbb{R}^{H_p \times K_a \times 16}$, where each multivector represents a predicted position, orientation, or scalar action component. This tensor is unpacked into individual multivectors corresponding to specific link or scalar properties at each time step, and then converted into standard geometric representations such as 3D positions, unit quaternions, and scalar values (e.g., for gripper control). Details of the conversion process from multivectors to standard representations are provided in §A.3. The resulting outputs can be passed to a controller or inverse kinematics solver to recover the final sequence of robot states.

A more in-depth explanation and design justification for this architecture is presented in §4.

Projective Geometric Algebra Transformer (P-GATr). For both the state encoder and action decoder in our architecture, we employ the P-GATr model and associated network primitives introduced by Brehmer et al. [2]. Structurally, P-GATr resembles a standard Transformer [4] with pre-layer normalization [38, 39]. Each of the N Transformer blocks in P-GATr includes an Equivariant Linear layer (Equi. Linear), Geometric Bilinear layers (Geo. Bilinear), Multivector Attention (GA Attn), a Scalar-Gated Gaussian Error Linear Unit (Gated GELU) [40], and an E(3)-Equivariant LayerNorm (Equi. LayerNorm). A detailed description of these components can be found in the original P-GATr paper by Brehmer et al. [2].

4 Architecture Design Choices and Details

In this section, we describe the network design choices and training procedure of hPGA-DP. In preliminary experiments, we initially employed P-GATr directly as the denoising network, aiming to leverage its strong geometric inductive bias. However, we observed that this naive integration resulted in impractically slow convergence, consistent with results in concurrent work by Zhong and Allen-Blanchette [37], which reports week-long training times. We hypothesize that this inefficiency stems from a fundamental mismatch in inductive priors: P-GATr is tailored for processing structured geometric data, whereas the objective of the denoising module is to reverse a stochastic process.

Based on this observation, we design hPGA-DP such that traditional architectures, such as Transformers or U-Nets, serve as the denoising backbone, while P-GATr is utilized as an encoder for observations and a decoder for actions. This allows the denoising process to operate in a latent space where geometric structure is learned implicitly through P-GATr, but without constraining the denoising network itself to a deterministic geometric bias.

Following standard diffusion frameworks [1, 5], we apply the forward noising process to the action latent space:

$$\mathbf{z}_{a,k} = \sqrt{\bar{\alpha}_k} \mathbf{z}_{a,0} + \sqrt{1 - \bar{\alpha}_k} \boldsymbol{\varepsilon}, \quad \boldsymbol{\varepsilon} \sim \mathcal{N}(0, \mathbf{I}), \quad (1)$$

where $\mathbf{z}_{a,k}$ denotes the noisy latent at denoising step k , $\mathbf{z}_{a,0}$ is the clean latent representation of the action sequence, $\bar{\alpha}_k$ is the cumulative signal retention factor from the noise scheduler that monotonically decreases as k increases, and $\boldsymbol{\varepsilon}$ is sampled from a standard Gaussian. During inference, $\mathbf{z}_{a,0}$

is generated by the denoising model. During training, we apply noise directly to ground-truth action multivector sequences, $\mathbf{x}_a^{t:t+H_p}$, to generate training samples.

The state encoder and denoising module ϵ_θ are trained to predict the added noise, with the following mean squared error loss:

$$\mathcal{L}_{\text{Encode\&Denoise}} = \|\epsilon_\theta(\mathbf{z}_{a,k}, \mathbf{z}_o, k) - \varepsilon\|^2.$$

where ϵ_θ takes as input the noisy latent $\mathbf{z}_{a,k}$ at timestep k , and is conditioned on the observation latent \mathbf{z}_o to predict the noise ε .

Although the state encoder and denoising module are jointly trained using the loss $\mathcal{L}_{\text{Encode\&Denoise}}$, the action decoder is intentionally excluded from this objective. This design choice stems from the fact that diffusion models are trained by sampling random denoising steps, where the model predicts noise at arbitrary points in the denoising trajectory in parallel. In contrast, inference proceeds sequentially through all denoising steps in an iterative manner. If the action decoder were used across all training steps, it would become entangled again with the denoising process, requiring it to decode from highly noisy action latents that are not suitable for the geometric inductive bias of P-GATr.

To address this problem, we restrict the decoder’s supervision to the final η fraction of denoising steps, where η is a threshold percentage to mask the loss for decoder. The threshold denoising step is calculated by:

$$K_{\text{thresh}} = K_{\text{max}} - \lfloor \eta \cdot K_{\text{max}} \rfloor, \quad (2)$$

where K_{max} is the total number of denoising steps and $\eta \in [0, 1]$ is a tunable parameter. We empirically show that this approach is robust to the choice of η in ablation studies. By limiting supervision to well-denoised action latents, the decoder learns to operate in a structured regime closer to what it encounters during inference, avoiding the need to decode from pure noise.

Since the denoising module ϵ_θ predicts the noise added to the clean latent, we first use its predicted noise $\hat{\varepsilon}$ to compute the estimated denoised action latent $\hat{\mathbf{z}}_{a,0}$ via the standard reverse process from Ho et al. [5]:

$$\hat{\mathbf{z}}_{a,0} = \frac{1}{\sqrt{\bar{\alpha}_k}} (\mathbf{z}_{a,k} - \sqrt{1 - \bar{\alpha}_k} \cdot \hat{\varepsilon}),$$

where $\bar{\alpha}_k$ is the cumulative signal retention factor at timestep k , which we also use for the forward noising process.

The decoder is then trained to reconstruct the ground-truth action multivector sequence $\mathbf{x}_a^{t:t+H_p}$ from $\hat{\mathbf{z}}_{a,0}$. The decoder loss is defined as:

$$\mathcal{L}_{\text{Decoder}} = \mathbb{1}_{\{k \geq K_{\text{thresh}}\}} \cdot \left\| D_\phi(\hat{\mathbf{z}}_{a,0}) - \mathbf{x}_a^{t:t+H_p} \right\|^2,$$

where D_ϕ denotes the action decoder, and $\mathbb{1}_{\{\cdot\}}$ is an indicator function that activates only when the current denoising step k exceeds the threshold K_{thresh} .

This staged supervision strategy preserves architectural modularity, leverages geometric inductive biases of PGA, and speeds up training by limiting the decoder’s learning signal to geometrically meaningful latents. The overall training objective of hPGA-DP combines both loss components:

$$\mathcal{L}_{\text{Total}} = \mathcal{L}_{\text{Encode\&Denoise}} + \mathcal{L}_{\text{Decoder}}.$$

5 Evaluation

5.1 Simulation Experiments

Experimental Settings. We evaluate the proposed hPGA-DP framework through simulation experiments and ablation studies across five Robosuite tasks [41], using a 7-DOF Panda Arm. As shown in the top row of Fig. 2, the tasks include: Lift (lift a red cube), Can (sort a can), Stack (stack a red cube on a green one), Square (insert a square nut), and Mug (place a mug into a drawer). Demonstrations for Lift and Can are sourced from Robomimic [42], while those for Stack, Square, and Mug

are generated using MimicGen [43]. Each dataset contains 200 trajectories, except Mug, which uses 300 due to its higher complexity.

We compare two hPGA-DP variants: hPGA-U and hPGA-T, which use U-Net and Transformer denoising modules, respectively. Baselines include U-Net, Transformer (Trans.), and P-GATr backbones without the encoder-denoiser-decoder structure. The U-Net and Transformer variants contain 24M and 35M parameters, respectively. For object pose input, we test both ground-truth state access (State) and 6D pose estimation using PRISM-DP [44] with FoundationPose [45], leveraging RGB, depth, and generated mesh inputs.

All models are implemented in PyTorch [46] and trained on a workstation with an AMD PRO 5975WX CPU, dual NVIDIA RTX 4090 GPUs, and 128GB RAM. Training schedules are: 80 epochs (Lift), 90 (Can), 30 (Stack), 120 (Square), and 100 (Mug). For all hPGA-DP variants, the maximum denoising step is set to $K_{\max} = 100$, and the action decoder loss is applied only during the final $\eta = 0.25$ portion of the denoising steps.

Each policy is evaluated over 50 rollouts, and success rate, which is defined as the fraction of successful trials, is reported as the primary performance metric, while the mean training time per epoch measured in seconds for each network across all tasks is reported as an indication of efficiency.

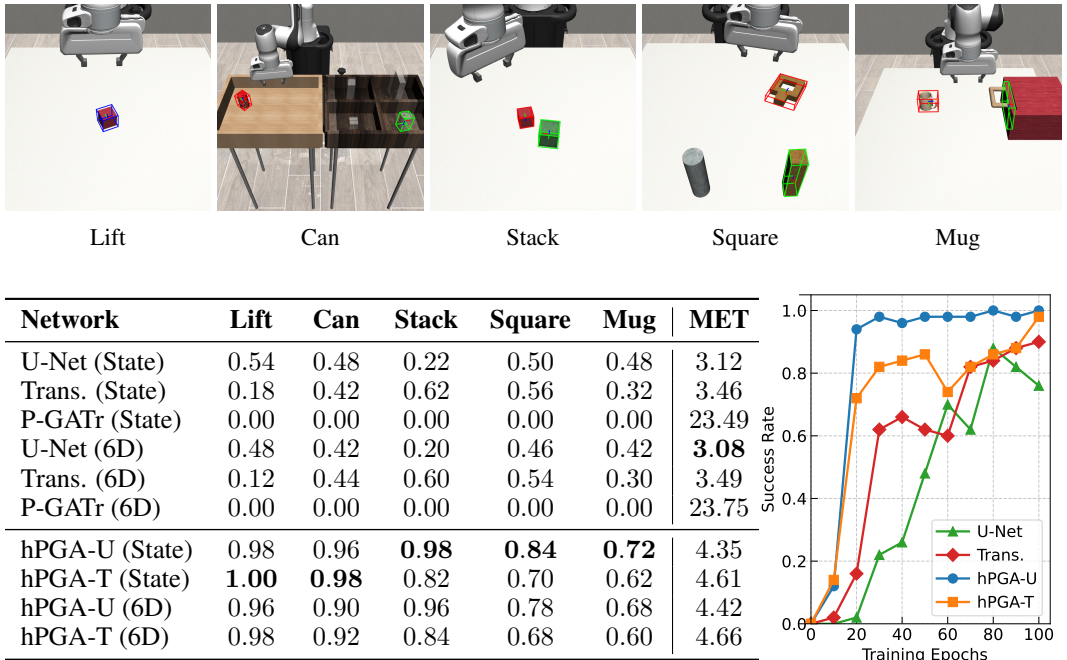


Figure 2: **Top**: simulation tasks in robosuite, with colored 3D bounding boxes indicating task-relevant objects. **Bottom left**: success rates for diffusion policies with different network backbones for various tasks, and mean epoch training time (MET) for each network on all tasks together. **Bottom right**: plot of success rate for state-based policies with U-Net, Transformer, hPGA-U, and hPGA-T for 100 training epochs of the Stack task.

Results. The results in Fig. 2 show that hPGA-DP, regardless of using U-Net or Transformer for denoising, consistently outperforms baseline policies that rely solely on these backbones. hPGA-DP achieves strong performance within 100 epochs on most tasks, with the exception of Mug, which involves multi-step interactions and requires more training. Notably, hPGA-U, despite having fewer parameters, often surpasses hPGA-T in performance.

hPGA-DP also demonstrates greater training efficiency. Despite that hPGA-DP takes more time to train per epoch according to the MET column of the bottom left table on Fig. 2, it requires many fewer training epochs to converge. For example, in the Stack task (bottom-right plot, Fig. 2), hPGA-

DP variants reach high success rates within about 30 epochs, while U-Net-only and Transformer-only baselines require roughly three times more training epochs to match this level.

Policies using P-GATr as the denoising network fail across all tasks due to extremely slow convergence. As corroborated by the concurrent work [37], training P-GATr for effective denoising requires at least seven days on high-end GPUs, rendering it far less practical than both hPGA-DP and standard diffusion backbones.

Ablation Studies. To further analyze the design of hPGA-DP, we conduct two ablation studies: (1) to identify an effective range for the action decoder loss masking threshold η , and (2) to evaluate whether the performance gains stem primarily from the encoder-denoiser-decoder layout. All experiments are conducted on the Stack task, which converges most rapidly among the benchmarks. Each configuration is evaluated over 5 trials, with 50 rollouts per trial. We report mean and standard deviation of the success rate.

For the η ablation, we test 10 values from 0.0 to 1.0 in increments of 0.1 for both hPGA-U and hPGA-T, using ground-truth object states. We additionally include two intermediate values in regions showing steep performance drops, resulting in 12 variants per model (top plot, Fig. 3). Results show that both hPGA-U and hPGA-T are robust to the choice of η : hPGA-U performs well for $\eta \in [0.05, 0.75]$, while hPGA-T maintains stable performance within $\eta \in [0.05, 0.95]$. The low variance across trials reflects consistency in training.

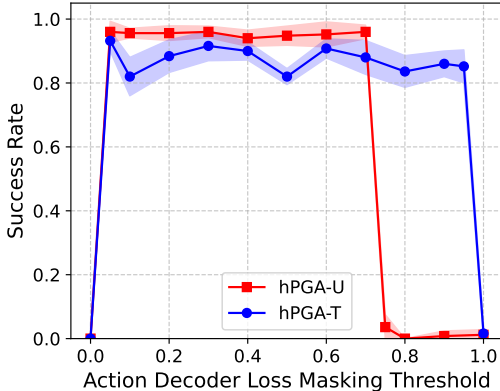
This robustness aligns with observations by Ho et al. [5], which suggest that most noise is removed in early denoising steps. Consequently, action latents quickly acquire a coarse geometric structure sufficient for effective decoder training, even if not yet executable. High values of η still provide meaningful gradients, while very low η limits decoder updates since most samples are excluded.

To evaluate the impact of network layout, we perform a second ablation by varying the encoder and decoder while keeping the denoiser fixed as either Transformer or U-Net. We compare three encoder-decoder types: MLP, Transformer, and P-GATr. The P-GATr variants correspond to hPGA-T and hPGA-U. MLP and Transformer are included due to their widespread use in prior works as encoder and decoder [47, 48, 49], while U-Net is typically only used as backbone [50, 51, 52]. For MLP and Transformer variants, we use standard MSE loss [1], as they do not operate on multivectors and thus do not require loss masking or η .

As shown in Fig.3, using MLP or Transformer as the encoder and decoder does not yield significant improvements over their baselines in Fig.2. This suggests that the gains from hPGA-DP arise not simply from its layout, but from the integration of P-GATr and its geometry-aware training strategy.

5.2 Real-World Experiments

Experimental Settings. To further evaluate hPGA-DP, we conduct real-world experiments using a dual-arm setup (top-left image, Fig. 4) consisting of two 7-DOF xArm7 robots mounted on 1-DOF linear actuators. One arm is equipped with an Intel RealSense D435i depth camera, while the other is fitted with a parallel gripper. The system operates in a look-at end-effector space, where



	<i>MLP</i>	<i>Trans.</i>	<i>P-GATr</i>
<u>U-Net</u>	0.24±0.06	0.26±0.04	0.96±0.02
<u>Trans.</u>	0.58±0.04	0.62±0.04	0.88±0.05

Figure 3: **Top:** Success rate of hPGA-DP under different decoder loss masking thresholds η , where solid line denotes the mean and shaded region indicates the standard deviation. **Bottom:** Performance of diffusion policies with various combinations of backbone (underlined) and *encoder & decoder* (italicized).

the camera’s orientation is excluded from the state-action space by dynamically adjusting it through inverse kinematics constraints to maintain focus on the gripper [53, 54].

We evaluate our approach on two real-world tasks, visualized in Fig. 4. The block stacking task (Block Stack.) requires placing a non-cuboid block onto another, while the drawer interaction task (Drawer Inter.) involves clearing a visual occlusion, retrieving a red cube, inserting it into a drawer, and closing the drawer. The blocks and drawer are 3D printed using meshes from Lee et al. [55] and Heo et al. [56], which are also used as ground-truth meshes for evaluation. Each task is trained on a dataset of 200 demonstration rollouts.

The evaluated conditions are the same as the simulation experiment with the exception of those that received ground-truth state information as that is not available in the real-world. Instead, all conditions inferred object poses using the same 6D pose estimation strategy employed in the simulation experiments—namely, PRISM-DP [44] with a Foundation-Pose backend [45]. An example of pose tracking results from a single frame is shown in the top-right panel of Fig. 4.

Training and inference are performed on the same workstation used for simulation. We report success rate and cumulative training time as performance metrics. Note that training time includes only the forward and backward passes during epoch training, excluding data loading and sampling overhead.

Results As shown in the table of Fig. 4, hPGA-DP achieves significantly higher success rates compared to other network backbones trained for the same number of epochs. While hPGA-DP requires more training time than Transformer and U-Net baselines, those baselines need to be trained for twice as many epochs to match hPGA-DP’s performance, which results in 21% to 36% higher total training time. These findings are consistent with simulation results, demonstrating that hPGA-DP offers superior performance and training efficiency over traditional diffusion backbones.

6 Discussion

In this work, we present hPGA-DP, a hybrid diffusion policy architecture that integrates P-GATr for encoding and decoding, while employing conventional U-Net or Transformer modules for denoising. To fully leverage the geometric inductive bias of P-GATr without incurring the high training cost of using it as a denoiser, we adopt a staged supervision strategy, which trains the action decoder only on geometrically coherent outputs after denoising. This approach retains the benefits of P-GATr’s geometric reasoning while maintaining practical training efficiency.

To our knowledge, this is the first work to successfully incorporate PGA into diffusion policies in a practical and scalable way. Our results demonstrate that embedding geometric inductive biases through PGA can significantly enhance policy learning, particularly in robotics where tasks are inherently spatial.



Network	Block		Drawer	
	SR	CT	SR	CT
U-Net	0.43	9.85	0.27	14.28
Trans.	0.37	12.03	0.40	15.87
P-GATr	0.00	92.42	0.00	119.63
hPGA-U	0.97	16.25	0.90	22.53
hPGA-T	0.93	17.69	0.87	26.81

Figure 4: **Top left:** the dual-arm system for real-world experiments. **Top right:** top and bottom row show the block stacking task and drawer interaction task respectively. **Bottom:** results for real-world experiments. SR: success rate, CT: cumulative training time measured in minutes.

Limitations. While hPGA-DP demonstrates promising initial results, it has several limitations suggesting future extensions. First, due to the nature of Projective Geometric Algebra (PGA), our method is restricted to using robot state and estimated 6D object poses as input conditions. It cannot directly operate on RGB images or point clouds. RGB data lacks inherent geometric structure and thus cannot be directly encoded as multivectors. Point clouds, while geometric, pose a challenge due to memory overhead: embedding each point into a 16-dimensional multivector leads to impractical memory usage. As a result, this approach is currently limited to rigid-body tasks with well-defined 6D poses, and cannot handle more complex phenomena such as soft-body dynamics or cloth manipulation—domains where image-based observation spaces may, in principle, offer more flexible representational capacity.

Also, although hPGA-DP converges in fewer epochs than traditional diffusion backbones, each epoch takes slightly longer to train. This inefficiency likely stems from our current PyTorch-based implementation, where the default backward pass may poorly handle the intricate blade-wise interactions in PGA. Optimizing the backward computation using lower-level frameworks such as Triton [57] could significantly improve per-epoch efficiency and overall training time.

In summary, while hPGA-DP outperforms conventional diffusion backbones in performance and convergence speed, addressing these limitations can further enhance its applicability and efficiency in solving robot learning tasks with strong built-in geometric priors.

References

- [1] C. Chi, Z. Xu, S. Feng, E. Cousineau, Y. Du, B. Burchfiel, R. Tedrake, and S. Song. Diffusion policy: Visuomotor policy learning via action diffusion. *The International Journal of Robotics Research*, page 02783649241273668, 2023.
- [2] J. Brehmer, P. De Haan, S. Behrends, and T. S. Cohen. Geometric algebra transformer. *Advances in Neural Information Processing Systems*, 36:35472–35496, 2023.
- [3] O. Ronneberger, P. Fischer, and T. Brox. U-net: Convolutional networks for biomedical image segmentation. In *Medical image computing and computer-assisted intervention–MICCAI 2015: 18th international conference, Munich, Germany, October 5–9, 2015, proceedings, part III 18*, pages 234–241. Springer, 2015.
- [4] A. Vaswani, N. Shazeer, N. Parmar, J. Uszkoreit, L. Jones, A. N. Gomez, Ł. Kaiser, and I. Polosukhin. Attention is all you need. *Advances in neural information processing systems*, 30, 2017.
- [5] J. Ho, A. Jain, and P. Abbeel. Denoising diffusion probabilistic models. *Advances in neural information processing systems*, 33:6840–6851, 2020.
- [6] A. Nichol, P. Dhariwal, A. Ramesh, P. Shyam, P. Mishkin, B. McGrew, I. Sutskever, and M. Chen. Glide: Towards photorealistic image generation and editing with text-guided diffusion models. *arXiv preprint arXiv:2112.10741*, 2021.
- [7] D. Podell, Z. English, K. Lacey, A. Blattmann, T. Dockhorn, J. Müller, J. Penna, and R. Rombach. Sdxl: Improving latent diffusion models for high-resolution image synthesis. *arXiv preprint arXiv:2307.01952*, 2023.
- [8] Y. Guo, C. Yang, A. Rao, Z. Liang, Y. Wang, Y. Qiao, M. Agrawala, D. Lin, and B. Dai. AnimateDiff: Animate your personalized text-to-image diffusion models without specific tuning. *arXiv preprint arXiv:2307.04725*, 2023.
- [9] A. Sridhar, D. Shah, C. Glossop, and S. Levine. Nomad: Goal masked diffusion policies for navigation and exploration. In *2024 IEEE International Conference on Robotics and Automation (ICRA)*, pages 63–70. IEEE, 2024.
- [10] D. Wang, C. Liu, F. Chang, and Y. Xu. Hierarchical diffusion policy: manipulation trajectory generation via contact guidance. *IEEE Transactions on Robotics*, 2025.
- [11] K. Kondo, A. Tagliabue, X. Cai, C. Tewari, O. Garcia, M. Espitia-Alvarez, and J. P. How. Cgd: Constraint-guided diffusion policies for uav trajectory planning. *arXiv preprint arXiv:2405.01758*, 2024.
- [12] Y. Ze, G. Zhang, K. Zhang, C. Hu, M. Wang, and H. Xu. 3d diffusion policy: Generalizable visuomotor policy learning via simple 3d representations. *arXiv preprint arXiv:2403.03954*, 2024.
- [13] D. Wang, S. Hart, D. Surovik, T. Kelestemur, H. Huang, H. Zhao, M. Yeatman, J. Wang, R. Walters, and R. Platt. Equivariant diffusion policy. *arXiv preprint arXiv:2407.01812*, 2024.
- [14] X. Sun, S. Yang, Y. Chen, F. Fan, Y. Liang, and D. Rakita. Dynamic rank adjustment in diffusion policies for efficient and flexible training. *arXiv preprint arXiv:2502.03822*, 2025.
- [15] M. Reuss, J. Pari, P. Agrawal, and R. Lioutikov. Efficient diffusion transformer policies with mixture of expert denoisers for multitask learning. *arXiv preprint arXiv:2412.12953*, 2024.
- [16] W. Peebles and S. Xie. Scalable diffusion models with transformers. In *Proceedings of the IEEE/CVF international conference on computer vision*, pages 4195–4205, 2023.

- [17] Z. Hou, T. Zhang, Y. Xiong, H. Pu, C. Zhao, R. Tong, Y. Qiao, J. Dai, and Y. Chen. Diffusion transformer policy. *arXiv preprint arXiv:2410.15959*, 2024.
- [18] Q. Wang, Y. Sun, E. Lu, Q. Zhang, and Y. Zeng. Mtdp: Modulated transformer diffusion policy model. *arXiv preprint arXiv:2502.09029*, 2025.
- [19] L. Dorst, D. Fontijne, and S. Mann. *Geometric algebra for computer science (revised edition): An object-oriented approach to geometry*. Morgan Kaufmann, 2009.
- [20] L. Dorst and S. De Keninck. A guided tour to the plane-based geometric algebra pga. *URL <https://bivector.net/PGA4CS.html>*, 2022.
- [21] M. Roelfs and S. De Keninck. Graded symmetry groups: plane and simple. *Advances in Applied Clifford Algebras*, 33(3):30, 2023.
- [22] L. Lechuga-Gutierrez, E. Macias-Garcia, G. Martínez-Terán, J. Zamora-Esquivel, and E. Bayro-Corrochano. Iterative inverse kinematics for robot manipulators using quaternion algebra and conformal geometric algebra. *Meccanica*, 57(6):1413–1428, 2022.
- [23] D. Zhu, Z. Zhang, and D. Li. A conformal geometric algebra method for inverse kinematics analysis of 6r robotic arm. *Journal of Mechanisms and Robotics*, pages 1–34, 2025.
- [24] O. Carbajal-Espinosa, L. Campos-Macías, and M. Díaz-Rodríguez. Fika: a conformal geometric algebra approach to a fast inverse kinematics algorithm for an anthropomorphic robotic arm. *Machines*, 12(1):78, 2024.
- [25] T. Löw and S. Calinon. Geometric algebra for optimal control with applications in manipulation tasks. *IEEE Transactions on Robotics*, 39(5):3586–3600, 2023.
- [26] C. Bilaloglu, T. Löw, and S. Calinon. Tactile ergodic control using diffusion and geometric algebra. *arXiv preprint arXiv:2402.04862*, 2024.
- [27] D. Ruhe, J. Brandstetter, and P. Forré. Clifford group equivariant neural networks. *Advances in Neural Information Processing Systems*, 36:62922–62990, 2023.
- [28] D. Ruhe, J. K. Gupta, S. De Keninck, M. Welling, and J. Brandstetter. Geometric clifford algebra networks. In *International Conference on Machine Learning*, pages 29306–29337. PMLR, 2023.
- [29] P. De Haan, T. Cohen, and J. Brehmer. Euclidean, projective, conformal: Choosing a geometric algebra for equivariant transformers. In *International Conference on Artificial Intelligence and Statistics*, pages 3088–3096. PMLR, 2024.
- [30] G. Sun and Y. Ding. An analytical method for sensitivity analysis of rigid multibody system dynamics using projective geometric algebra. *Journal of Computational and Nonlinear Dynamics*, 18(11), 2023.
- [31] G. Sun and Y. Ding. High-order inverse dynamics of serial robots based on projective geometric algebra. *Multibody System Dynamics*, 59(3):337–362, 2023.
- [32] Q. Liu and W. Cao. Geometric algebra graph neural network for cross-domain few-shot classification. *Applied Intelligence*, 52(11):12422–12435, 2022.
- [33] J. Zhong and W. Cao. Geometric algebra-based multiview interaction networks for 3d human motion prediction. *Pattern Recognition*, 138:109427, 2023.
- [34] J. Brehmer, V. Bresó, P. de Haan, T. Plehn, H. Qu, J. Spinner, and J. Thaler. A lorentz-equivariant transformer for all of the lhc. *arXiv preprint arXiv:2411.00446*, 2024.

- [35] J. Suk, B. Imre, and J. M. Wolterink. Lab-gatr: geometric algebra transformers for large biomedical surface and volume meshes. In *International Conference on Medical Image Computing and Computer-Assisted Intervention*, pages 185–195. Springer, 2024.
- [36] K. L. K. Lee, C. Gonzales, M. Spellings, M. Galkin, S. Miret, and N. Kumar. Towards foundation models for materials science: The open matsci ml toolkit. In *Proceedings of the SC’23 Workshops of the International Conference on High Performance Computing, Network, Storage, and Analysis*, pages 51–59, 2023.
- [37] T. Zhong and C. Allen-Blanchette. Gagrasp: Geometric algebra diffusion for dexterous grasping. *arXiv preprint arXiv:2503.04123*, 2025.
- [38] R. Xiong, Y. Yang, D. He, K. Zheng, S. Zheng, C. Xing, H. Zhang, Y. Lan, L. Wang, and T. Liu. On layer normalization in the transformer architecture. In *International conference on machine learning*, pages 10524–10533. PMLR, 2020.
- [39] A. Baevski and M. Auli. Adaptive input representations for neural language modeling. In *International Conference on Learning Representations*.
- [40] D. Hendrycks and K. Gimpel. Gaussian error linear units (gelus). *arXiv preprint arXiv:1606.08415*, 2016.
- [41] Y. Zhu, J. Wong, A. Mandlekar, R. Martín-Martín, A. Joshi, S. Nasiriany, and Y. Zhu. robosuite: A modular simulation framework and benchmark for robot learning. *arXiv preprint arXiv:2009.12293*, 2020.
- [42] A. Mandlekar, D. Xu, J. Wong, S. Nasiriany, C. Wang, R. Kulkarni, L. Fei-Fei, S. Savarese, Y. Zhu, and R. Martín-Martín. What matters in learning from offline human demonstrations for robot manipulation. In *Conference on Robot Learning (CoRL)*, 2021.
- [43] A. Mandlekar, S. Nasiriany, B. Wen, I. Akinola, Y. Narang, L. Fan, Y. Zhu, and D. Fox. Mimicgen: A data generation system for scalable robot learning using human demonstrations. *arXiv preprint arXiv:2310.17596*, 2023.
- [44] X. Sun, Y. Chen, and D. Rakita. Prism-dp: Spatial pose-based observations for diffusion-policies via segmentation, mesh generation, and pose tracking. *arXiv preprint arXiv:2504.20359*, 2025.
- [45] B. Wen, W. Yang, J. Kautz, and S. Birchfield. Foundationpose: Unified 6d pose estimation and tracking of novel objects. In *Proceedings of the IEEE/CVF Conference on Computer Vision and Pattern Recognition*, pages 17868–17879, 2024.
- [46] A. Paszke, S. Gross, F. Massa, A. Lerer, J. Bradbury, G. Chanan, T. Killeen, Z. Lin, N. Gimelshein, L. Antiga, A. Desmaison, A. Kopf, E. Yang, Z. DeVito, M. Raison, A. Tejani, S. Chilamkurthy, B. Steiner, L. Fang, J. Bai, and S. Chintala. Pytorch: An imperative style, high-performance deep learning library. In *Advances in Neural Information Processing Systems 32*, pages 8024–8035. Curran Associates, Inc., 2019. URL <http://papers.neurips.cc/paper/9015-pytorch-an-imperative-style-high-performance-deep-learning-library.pdf>.
- [47] Y. Wu, X. Sun, I. Spasojevic, and V. Kumar. Deep learning for optimization of trajectories for quadrotors. *IEEE Robotics and Automation Letters*, 9(3):2479–2486, 2024.
- [48] A. Loquercio, E. Kaufmann, R. Ranftl, M. Müller, V. Koltun, and D. Scaramuzza. Learning high-speed flight in the wild. *Science Robotics*, 6(59):eabg5810, 2021.
- [49] A. Dosovitskiy, L. Beyer, A. Kolesnikov, D. Weissenborn, X. Zhai, T. Unterthiner, M. Dehghani, M. Minderer, G. Heigold, S. Gelly, et al. An image is worth 16x16 words: Transformers for image recognition at scale. *arXiv preprint arXiv:2010.11929*, 2020.

- [50] N. Sharma, S. Gupta, D. Koundal, S. Alyami, H. Alshahrani, Y. Asiri, and A. Shaikh. U-net model with transfer learning model as a backbone for segmentation of gastrointestinal tract. *Bioengineering*, 10(1):119, 2023.
- [51] C. Si, Z. Huang, Y. Jiang, and Z. Liu. Freeu: Free lunch in diffusion u-net. In *Proceedings of the IEEE/CVF Conference on Computer Vision and Pattern Recognition*, pages 4733–4743, 2024.
- [52] I. Mitsouras, E. Tsonis, P. Tzouveli, and A. Voulodimos. U-sketch: An efficient approach for sketch to image diffusion models. *arXiv preprint arXiv:2403.18425*, 2024.
- [53] X. Sun, F. Fan, Y. Chen, and D. Rakita. A comparative study on state-action spaces for learning viewpoint selection and manipulation with diffusion policy. *arXiv preprint arXiv:2409.14615*, 2024.
- [54] D. Rakita, B. Mutlu, and M. Gleicher. An autonomous dynamic camera method for effective remote teleoperation. In *Proceedings of the 2018 ACM/IEEE International Conference on Human-Robot Interaction*, pages 325–333, 2018.
- [55] A. X. Lee, C. M. Devin, Y. Zhou, T. Lampe, K. Bousmalis, J. T. Springenberg, A. Byravan, A. Abdolmaleki, N. Gileadi, D. Khosid, et al. Beyond pick-and-place: Tackling robotic stacking of diverse shapes. In *5th Annual Conference on Robot Learning*, 2021.
- [56] M. Heo, Y. Lee, D. Lee, and J. J. Lim. Furniturebench: Reproducible real-world benchmark for long-horizon complex manipulation. *The International Journal of Robotics Research*, page 02783649241304789, 2023.
- [57] P. Tillet, H.-T. Kung, and D. Cox. Triton: an intermediate language and compiler for tiled neural network computations. In *Proceedings of the 3rd ACM SIGPLAN International Workshop on Machine Learning and Programming Languages*, pages 10–19, 2019.

A Appendix

A.1 Geometric Algebra Primer

This subsection provides a high-level overview of Geometric Algebra (GA), the mathematical framework underlying our work. This overview is not intended to be comprehensive; rather, it serves as a convenient introduction or reference for key ideas relevant to our approach. For a more complete treatment of GA, we refer the reader to Dorst et al. [19].

Vector Space and Basis Elements. GA is an algebra constructed from an n -dimensional vector space V . The space V has n basis elements, denoted $\mathbf{e}_1, \mathbf{e}_2, \dots, \mathbf{e}_n$. A dot product is defined between all basis elements, i.e., $\mathbf{e}_i \cdot \mathbf{e}_j$ is specified for all $i, j \in \{1, \dots, n\}$. Importantly, the dot product of a basis vector with itself need not be strictly positive in GA—i.e., $\mathbf{e}_i \cdot \mathbf{e}_i$ may be negative. Throughout our primer explanations, we will assume an orthogonal basis, i.e., $\mathbf{e}_i \cdot \mathbf{e}_j = 0$ if $i \neq j$. While this is not a strict requirement in GA, it is common and convenient in most cases.

Using the definitions above, we can create arbitrary vector objects using a linear combination of basis elements:

$$x_1\mathbf{e}_1 + x_2\mathbf{e}_2 + \dots + x_n\mathbf{e}_n,$$

where $x_1, \dots, x_n \in \mathbb{R}$. Also, we can recover the dot product between arbitrary vector objects by using distributivity:

$$\begin{aligned} (x_1\mathbf{e}_1 + x_2\mathbf{e}_2 + \dots + x_n\mathbf{e}_n) \cdot (y_1\mathbf{e}_1 + y_2\mathbf{e}_2 + \dots + y_n\mathbf{e}_n) = \\ x_1y_1(\mathbf{e}_1 \cdot \mathbf{e}_1) + x_2y_2(\mathbf{e}_2 \cdot \mathbf{e}_2) + \dots + x_ny_n(\mathbf{e}_n \cdot \mathbf{e}_n) \end{aligned}$$

Signature. Throughout GA, it is most common for basis elements to square to 1, -1 , or 0, i.e., $\mathbf{e}_i \cdot \mathbf{e}_i \in \{1, -1, 0\}$. The notation $\mathbb{R}^{p,q,r}$ is referred to as the *metric signature* of the GA, signifying that p basis vectors square to 1, q basis vectors square to -1 , and r basis vectors square to 0. If the ambient vector space is of size n , then $p+q+r = n$. The geometric algebra corresponding to $\mathbb{R}^{p,q,r}$, denoted by $\mathbb{G}^{p,q,r}$, includes not only the metric structure but also the full set of operations and representations, such as multivectors and the geometric product, defined over that space (explained more below).

Outer Product. The vector expression $x_1\mathbf{e}_1 + x_2\mathbf{e}_2 + \cdots + x_n\mathbf{e}_n$ defines a direction in n -dimensional space. The set of all scalar multiples $\alpha(x_1\mathbf{e}_1 + x_2\mathbf{e}_2 + \cdots + x_n\mathbf{e}_n)$, where $\alpha \in \mathbb{R}$, forms a *one-dimensional subspace*—that is, a line through the origin oriented along this vector.

In Geometric Algebra (GA), it is possible to construct mathematical objects that represent *higher-dimensional subspaces*. An operation called the *outer product* (also known as the wedge product), denoted as \wedge , builds these higher-dimensional objects. For example, if we consider $\mathbf{x} = (x_1\mathbf{e}_1 + x_2\mathbf{e}_2 + \cdots + x_n\mathbf{e}_n)$ and $\mathbf{y} = (y_1\mathbf{e}_1 + y_2\mathbf{e}_2 + \cdots + y_n\mathbf{e}_n)$, the expression

$$\mathbf{x} \wedge \mathbf{y}$$

represents the two-dimensional planar subspace spanned by its two vector operands. Such an object is called a *bivector*. Similarly, incorporating a third vector, \mathbf{z} , yields

$$\mathbf{x} \wedge \mathbf{y} \wedge \mathbf{z},$$

which defines a *trivector* representing a three-dimensional subspace spanned by its vector operands.

By repeatedly applying the outer product, one can construct higher-dimensional subspace elements known as k -blades, where k denotes the number of vectors combined.

A k -blade possess both a *weight* and an *orientation*. The weight corresponds to the volume of the parallelepiped spanned by the vectors in the wedge product. Multiplying a k -blade by a scalar simply scales its weight. The orientation captures the handedness of the subspace, indicating whether it is positively or negatively oriented, depending on the ordering of its constituent vectors. Swapping the order of two vector operands reverses the orientation, i.e.,

$$\mathbf{x} \wedge \mathbf{y} = -\mathbf{y} \wedge \mathbf{x}.$$

Two k -blades are considered equivalent if they span the same subspace, have the same weight, and have the same orientation.

Importantly, a vector wedged with a scalar multiple of itself is zero, i.e., $\mathbf{x} \wedge \alpha\mathbf{x} = 0$. Thus, the largest k -blade that an n -dimensional space can hold is one with three vectors wedged together, as everything larger will no longer be linearly independent and will collapse to zero.

For a more rigorous treatment of the outer product and k -blades, we refer the reader to Dorst et al. [19].

Grade. The grade of a k -blade is the dimensionality of its spanning subspace. For instance, a 1-blade has grade 1, a 2-blade has grade 2, etc. A k -blade of grade 0 is simply a scalar.

Multivectors. A multivector is a linear combination of k -blades of different grades. The grade of each k -blade term ranges from 0 (scalars) up to n , the dimension of the underlying vector space.

The basis for the space of all multivectors in n -dimensional space consists of all distinct outer products (wedge products) of the basis vectors, called *basis blades*. These span all grades from 0 to n and collectively form a complete basis for the multivector space. For instance, the basis of the space of multivectors in 3-dimensional space is

$$\left\{ \underbrace{1}_{\text{scalars}}, \underbrace{\mathbf{e}_1, \mathbf{e}_2, \mathbf{e}_3}_{\text{vectors}}, \underbrace{(\mathbf{e}_1 \wedge \mathbf{e}_2), (\mathbf{e}_2 \wedge \mathbf{e}_3), (\mathbf{e}_1 \wedge \mathbf{e}_3)}_{\text{bivectors}}, \underbrace{(\mathbf{e}_1 \wedge \mathbf{e}_2 \wedge \mathbf{e}_3)}_{\text{trivectors}} \right\}.$$

This basis is often abbreviated using a compact notation that omits the wedge symbols and combines indices:

$$\left\{ \underbrace{1}_{\text{scalars}}, \underbrace{\mathbf{e}_1, \mathbf{e}_2, \mathbf{e}_3}_{\text{vectors}}, \underbrace{\mathbf{e}_{12}, \mathbf{e}_{23}, \mathbf{e}_{13}}_{\text{bivectors}}, \underbrace{\mathbf{e}_{123}}_{\text{trivectors}} \right\}.$$

The total number of k -blades in the basis of an n -dimensional space of multivectors is $\sum_{k=0}^n \binom{n}{k} = 2^n$. A full multivector when $n = 3$ can be written out as

$$x_0 + x_1 \mathbf{e}_1 + x_2 \mathbf{e}_2 + x_3 \mathbf{e}_3 + x_{12} \mathbf{e}_{12} + x_{23} \mathbf{e}_{23} + x_{13} \mathbf{e}_{13} + x_{123} \mathbf{e}_{123},$$

where all x objects denote scalar coefficients in the linear combination.

Geometric Product. The geometric product is the foundational operation in Geometric Algebra, unifying and extending familiar concepts like the dot and cross products into a single, consistent framework. It allows for the algebraic combination of vectors in a way that captures both their magnitude-based interactions (via the dot product) and the oriented subspaces they span (via the wedge product). This unified operation enables concise expressions of geometric transformations, projections, and reflections in any dimension. In this primer, we focus on the practical mechanics of using the geometric product; for a deeper treatment of its theoretical foundations and broader applications, we refer the reader to Dorst et al. [19].

The geometric product is defined by a single central formula that combines the dot product and the outer product:

$$\mathbf{xy} = \mathbf{x} \cdot \mathbf{y} + \mathbf{x} \wedge \mathbf{y},$$

where the geometric product is indicated by writing the two vectors with no space between them. Here, \mathbf{x} and \mathbf{y} are standard vectors (1-blades).

Note that the geometric product of a vector with itself reduces to the dot product, since the outer product vanishes: $\mathbf{xx} = \mathbf{x}^2 = \mathbf{x} \cdot \mathbf{x}$. Conversely, the geometric product of two orthogonal vectors reduces to their outer product, as the dot product becomes zero. This is particularly useful when working with basis vectors, which are typically orthogonal—for example, $\mathbf{e}_1 \mathbf{e}_2 = \mathbf{e}_1 \wedge \mathbf{e}_2 = \mathbf{e}_{12}$.

The geometric product can be used to represent a variety of spatial transformations. For example, if $\mathbf{a} = a_1 \mathbf{e}_1 + a_2 \mathbf{e}_2 + a_3 \mathbf{e}_3$ is a unit vector and $\mathbf{x} = x_1 \mathbf{e}_1 + x_2 \mathbf{e}_2 + x_3 \mathbf{e}_3$ is another vector, then the expression \mathbf{axa}^{-1} represents the reflection of \mathbf{x} through the plane perpendicular to \mathbf{a} . The geometric product inverse of a vector \mathbf{a}^{-1} is defined in GA as $\mathbf{a}^{-1} = \frac{\mathbf{a}}{\|\mathbf{a}\|^2}$, assuming $\mathbf{a} \neq \mathbf{0}$. This same pattern can be used to create rotations, simply applying another reflection.

Cayley Table. The geometric product identities introduced above can be organized into a reference structure known as a Cayley table, which tabulates the geometric product between all basis elements in the space of multivectors. For example, consider the multivector basis of $\mathbb{G}_{2,0,0}$:

$$\left\{ \underbrace{1}_{\text{scalars}}, \underbrace{\mathbf{e}_1, \mathbf{e}_2}_{\text{vectors}}, \underbrace{\mathbf{e}_{12}}_{\text{bivectors}} \right\}.$$

Using this basis, the geometric product between any pair of basis elements can be recorded in the following Cayley table (generated at bivector.net):

1	e_1	e_2	e_{12}
e_1	1	e_{12}	e_2
e_2	$-e_{12}$	1	$-e_1$
e_{12}	$-e_2$	e_1	-1

Figure 5: Cayley Table for $\mathbb{G}_{2,0,0}$

In this table, each entry represents the geometric product of the row label (left operand) with the column label (right operand). These tables provide a compact and efficient way to compute geometric products between arbitrary multivectors by applying distributivity across terms.

A.2 Projective Geometric Algebra Primer

Standard Geometric Algebra, covered above, provides a powerful framework for representing spatial operations such as projections, reflections, and rotations. However, it operates in a homogeneous (linear) setting, meaning all subspaces and operations are defined relative to the origin. This makes it ill-suited for representing affine transformations, such as translations, or geometric objects with positional offsets.

Projective Geometric Algebra (PGA) addresses this limitation by extending GA to incorporate projective and affine geometry. It enables the representation of points, lines, and planes in arbitrary positions, as well as transformations such as translations and rotations. As a result, PGA supports the two types of geometric entities most relevant to this work: positions and orientations.

In this subsection, we provide an overview of Projective Geometric Algebra (PGA). As with the preceding discussion of GA, this overview is not intended to be comprehensive, but rather to serve as a convenient introduction and reference for key concepts relevant to our approach. For a more complete treatment of PGA, we refer the reader to Dorst et al. [19].

Metric Signature for 3D PGA. The form of Projective Geometric Algebra (PGA) used in this work models 3D space, but it operates within a 4D representational space. The corresponding metric signature is $\mathbb{R}^{3,0,1}$, which gives rise to the geometric algebra $\mathbb{G}_{3,0,1}$. This space includes a single null basis element, denoted e_0 , which satisfies $e_0^2 = 0$.

Multivectors in $\mathbb{G}_{3,0,1}$. The basis for the space of multivectors in $\mathbb{G}_{3,0,1}$ is

$$\left\{ \underbrace{1}_{\text{scalars}}, \underbrace{e_0, e_1, e_2, e_3}_{\text{vectors}}, \underbrace{e_{01}, e_{02}, e_{03}, e_{12}, e_{13}, e_{23}}_{\text{bivectors}}, \underbrace{e_{012}, e_{013}, e_{023}, e_{123}}_{\text{trivectors}}, \underbrace{e_{0123}}_{\text{quadvectors}} \right\},$$

so a generic multivector in this space is written as following:

$$x_s + x_0 e_0 + x_1 e_1 + x_2 e_2 + x_3 e_3 + x_{01} e_{01} + x_{02} e_{02} + x_{03} e_{03} + x_{12} e_{12} + x_{13} e_{13} + x_{23} e_{23} + x_{012} e_{012} + x_{013} e_{013} + x_{023} e_{023} + x_{123} e_{123} + x_{0123} e_{0123}$$

Cayley table for 3D PGA. The Cayley table for 3D PGA, generated at bivector.net, is illustrated in Figure 6.

Distinction between points and directions. One of the primary roles of the extra basis element e_0 in PGA is to enable a mathematical distinction between *points* and *directions*. This distinction is essential for representing translations as algebraic operations within the algebra, something that standard Geometric Algebra does not support directly. In contrast, both standard Geometric Algebra and linear algebra use one-dimensional vector representations that conflate points and directions, relying on external context to determine whether a vector refers to a location or a direction in space.

In 3D PGA, a finite point \mathbf{x} is typically represented as:

$$\mathbf{x} = e_0 + x_1 e_1 + x_2 e_2 + x_3 e_3.$$

1	e_0	e_1	e_2	e_3	e_{01}	e_{02}	e_{03}	e_{12}	e_{31}	e_{23}	e_{021}	e_{013}	e_{032}	e_{123}	e_{0123}
e_0	0	e_{01}	e_{02}	e_{03}	0	0	0	$-e_{021}$	$-e_{013}$	$-e_{032}$	0	0	0	e_{0123}	0
e_1	$-e_{01}$	1	e_{12}	$-e_{31}$	$-e_0$	e_{021}	$-e_{013}$	e_2	$-e_3$	e_{123}	e_{02}	$-e_{03}$	e_{0123}	e_{23}	e_{032}
e_2	$-e_{02}$	$-e_{12}$	1	e_{23}	$-e_{021}$	$-e_0$	e_{032}	$-e_1$	e_{123}	e_3	$-e_{01}$	e_{0123}	e_{03}	e_{31}	e_{013}
e_3	$-e_{03}$	e_{31}	$-e_{23}$	1	e_{013}	$-e_{032}$	$-e_0$	e_{123}	e_1	$-e_2$	e_{0123}	e_{01}	$-e_{02}$	e_{12}	e_{021}
e_{01}	0	e_0	$-e_{021}$	e_{013}	0	0	0	e_{02}	$-e_{03}$	e_{0123}	0	0	0	$-e_{032}$	0
e_{02}	0	e_{021}	e_0	$-e_{032}$	0	0	0	$-e_{01}$	e_{0123}	e_{03}	0	0	0	$-e_{013}$	0
e_{03}	0	$-e_{013}$	e_{032}	e_0	0	0	0	e_{0123}	e_{01}	$-e_{02}$	0	0	0	$-e_{021}$	0
e_{12}	$-e_{021}$	$-e_2$	e_1	e_{123}	$-e_{02}$	e_{01}	e_{0123}	-1	e_{23}	$-e_{31}$	e_0	e_{032}	$-e_{013}$	$-e_3$	$-e_{03}$
e_{31}	$-e_{013}$	e_3	e_{123}	$-e_1$	e_{03}	e_{0123}	$-e_{01}$	$-e_{23}$	-1	e_{12}	$-e_{032}$	e_0	e_{021}	$-e_2$	$-e_{02}$
e_{23}	$-e_{032}$	e_{123}	$-e_3$	e_2	e_{0123}	$-e_{03}$	e_{02}	e_{31}	$-e_{12}$	-1	e_{013}	$-e_{021}$	e_0	$-e_1$	$-e_{01}$
e_{021}	0	e_{02}	$-e_{01}$	$-e_{0123}$	0	0	0	e_0	e_{032}	$-e_{013}$	0	0	0	e_{03}	0
e_{013}	0	$-e_{03}$	$-e_{0123}$	e_{01}	0	0	0	$-e_{032}$	e_0	e_{021}	0	0	0	e_{02}	0
e_{032}	0	$-e_{0123}$	e_{03}	$-e_{02}$	0	0	0	e_{013}	$-e_{021}$	e_0	0	0	0	e_{01}	0
e_{123}	$-e_{0123}$	e_{23}	e_{31}	e_{12}	e_{032}	e_{013}	e_{021}	$-e_3$	$-e_2$	$-e_1$	$-e_{03}$	$-e_{02}$	$-e_{01}$	-1	e_0
e_{0123}	0	$-e_{032}$	$-e_{013}$	$-e_{021}$	0	0	0	$-e_{03}$	$-e_{02}$	$-e_{01}$	0	0	0	$-e_0$	0

Figure 6: Cayley Table for 3D PGA

This encodes a point in Euclidean space with coordinates (x_1, x_2, x_3) , where the e_0 term encodes the ideal (or “at infinity”) direction component. The presence of e_0 distinguishes finite points from directions: if the e_0 term is omitted, the multivector instead represents a direction or a point at infinity.

PGA uses homogeneous coordinates, so multivectors that are scalar multiples of each other represent the same point:

$$\lambda(e_0 + x_1e_1 + x_2e_2 + x_3e_3) \sim e_0 + x_1e_1 + x_2e_2 + x_3e_3 \quad \text{for all } \lambda \neq 0.$$

This equivalence under scalar multiplication means that PGA points form an equivalence class of representatives, much like in projective geometry.

The scalar coefficient on the point representation—i.e., the multiplier λ —is referred to as the *weight* of the point. This weight does not affect the location of the point in space but can be meaningful in weighted computations, such as in interpolation or when accumulating mass-like quantities.

In contrast, a *direction* in PGA is represented without a e_0 component, such as:

$$\mathbf{v} = v_1e_1 + v_2e_2 + v_3e_3.$$

While the full geometric story is beyond the scope of this primer, such elements represent “points at infinity”, i.e., points with zero weights and, hence, attempting to normalize them would send the point infinitely far in their given direction. These elements are used to model directions, ideal lines, and translations. They are not affected by translations in space, which distinguishes them algebraically and geometrically from finite points.

A.3 Projective Geometric Algebra Conversions

In this subsection, we present conversions between standard spatial representations and their corresponding multivector forms in 3D Projective Geometric Algebra (PGA).

Scalar

$$s \in \mathbb{R} \iff s + 0e_0 + 0e_1 + 0e_2 + 0e_3 + 0e_{01} + 0e_{02} + 0e_{03} + 0e_{12} + 0e_{13} + 0e_{23} + 0e_{012} + 0e_{013} + 0e_{023} + 0e_{123} + 0e_{0123}$$

Direction

$$\begin{bmatrix} v_1 \\ v_2 \\ v_3 \end{bmatrix} \in \mathbb{R}^3 \iff 0 + 0\mathbf{e}_0 + v_1\mathbf{e}_1 + v_2\mathbf{e}_2 + v_3\mathbf{e}_3 + 0\mathbf{e}_{01} + 0\mathbf{e}_{02} + 0\mathbf{e}_{03} + 0\mathbf{e}_{12} + 0\mathbf{e}_{13} + 0\mathbf{e}_{23} + 0\mathbf{e}_{012} + 0\mathbf{e}_{013} + 0\mathbf{e}_{023} + 0\mathbf{e}_{123} + 0\mathbf{e}_{0123}$$

Position/ Point

$$\begin{bmatrix} x_1 \\ x_2 \\ x_3 \end{bmatrix} \in \mathbb{R}^3 \iff 0 + 0\mathbf{e}_0 + 0\mathbf{e}_1 + 0\mathbf{e}_2 + 0\mathbf{e}_3 + 0\mathbf{e}_{01} + 0\mathbf{e}_{02} + 0\mathbf{e}_{03} + 0\mathbf{e}_{12} + 0\mathbf{e}_{13} + 0\mathbf{e}_{23} - x_3\mathbf{e}_{012} + x_2\mathbf{e}_{013} - x_1\mathbf{e}_{023} + \mathbf{e}_{123} + 0\mathbf{e}_{0123}$$

(Note that this is the dual representation of the point form described above. While mathematically equivalent, we adopt this convention in our work to remain consistent with the work by Brehmer et al. [2]).

Orientation as Unit Quaternion

$$w + x\mathbf{i} + y\mathbf{j} + z\mathbf{k} \in \mathbb{H}_1 \iff w + 0\mathbf{e}_0 + 0\mathbf{e}_1 + 0\mathbf{e}_2 + 0\mathbf{e}_3 + 0\mathbf{e}_{01} + 0\mathbf{e}_{02} + 0\mathbf{e}_{03} - z\mathbf{e}_{12} + y\mathbf{e}_{13} - x\mathbf{e}_{23} + 0\mathbf{e}_{012} + 0\mathbf{e}_{013} + 0\mathbf{e}_{023} + 0\mathbf{e}_{123} + 0\mathbf{e}_{0123}$$